Engineering Geology 118 (2011) 110–121

Contents lists available at ScienceDirect

Engineering Geology

journal homepage: www.elsevier.com/locate/enggeo

The pore system of sedimentary rocks as a key factor in the durability of building materials

E. Molina [a], G. Cultrone [a,*], E. Sebastián [a], F.J. Alonso [b], L. Carrizo [b], J. Gisbert [c], O. Buj [c]

[a] Departamento de Mineralogía y Petrología, Facultad de Ciencias, Universidad de Granada, Spain
[b] Departamento de Geología, Área de Petrología y Geoquímica, Universidad de Oviedo, Spain
[c] Departamento de Ciencias de la Tierra, Facultad de Ciencias, Universidad de Zaragoza, Spain

ARTICLE INFO

Article history:
Received 23 June 2010
Received in revised form 18 January 2011
Accepted 29 January 2011
Available online 22 Febuary 2011

Keywords:
Sedimentary stones
Pore system characterization
Accelerated decay tests

ABSTRACT

We studied the pore system of six different types of sedimentary stone (two limestones, two sandstones, one dolostone and one travertine). Techniques based on the direct observation of the pore system (optical and scanning electron microscopes, digital image analysis) were combined with others used for indirect characterization (mercury intrusion porosimetry, N_2 adsorption, hydric tests, and vapour permeability). In addition, we performed accelerated decay tests to determine the durability of the stones and to check the consistency of the results obtained in the pore system study. Digital image analysis allowed us to calculate the pore size distribution and the total porosity. Digital image analysis always gave higher values for total porosity than those determined by porosimetry and hydric tests, which only measure open porosity. The density values were congruent with the mineralogy of the stones. The stone that obtained the best results in the various tests in terms of its petrophysical parameters was dolostone, while the worst performance was by one of the two limestones. These results were confirmed by the decay tests. The combined use of these different techniques gave us an accurate interpretation of the pore systems of the six different stones, and also enabled us to correct misleading interpretations caused by the limitations of using one single technique. Our findings also provide useful information to help prevent the decay of these stones.

1. Introduction

Every stone is composed of minerals and empty spaces. These empty spaces are normally pores or fissures, the volume and distribution of which strongly affect the behaviour of stones over time (Lazzarini and Laurenzi Tabasso, 1986; Rodríguez Navarro, 2003; Charola, 2004). Pores and fissures are the natural paths by which water flows through the material, thereby enhancing biological, physical and chemical weathering processes (Dunning and Huf, 1983; Franzen, 2004). For this reason it is of paramount importance to find out more about the porosity of the stones, in its broadest sense, in order to understand why and how to prevent or at least minimize damage to them (Esbert et al., 2008).

Vos (1978) distinguished three components in a porous material: the solid part of the material, the open pores (i.e., those accessible to water and other fluids) and the closed pores (which water cannot penetrate). Total porosity is the sum of open porosity and closed porosity, but open porosity is normally of more interest than total porosity since the former is actively involved in the hydric behaviour of stones (Alonso et al., 1987a,b). To this end, Whiteley et al. (1977) demonstrated that the open porosity of stones and their effective pore size is affected by the movement of water, basing their research on the comparison of pore size distribution values of various building materials collected from the literature.

To underline the effect of the pore system on the behaviour of stones, Ordoñez et al. (1994, 1997) defined a durability dimensional estimator on the basis of pore size distribution curves of porous limestones determined by means of mercury intrusion porosimetry. More recently, Benavente et al. (2004) introduced a new petrophysical durability estimator based both on the pore structure and the strength of stones, and found that this parameter was well correlated to the weathering produced by salt crystallization.

Although some of the pores and fissures are visible to the naked eye, the complexity and the nature of porosity (i.e., geometry, size, specific surface area, and grade of connection) can only be appreciated with precise measurements (Hall and Hoff, 2002). Most of the analytical techniques used to characterize the pore system are well established, but conflicting results are often obtained when these techniques are used in isolation.

For example, the pressure–volume hysteresis curves of similar stones obtained by mercury intrusion porosimetry were considered sufficiently sensitive to distinguish different degrees of durability (Robertson, 1982). However, this technique has been questioned as a reliable tool for determining durability indexes, at least in cement-

* Corresponding author. Tel.: +34 958 240077; fax: +34 958 243368.
E-mail address: cultrone@ugr.es (G. Cultrone).

0013-7952/$ – see front matter © 2011 Elsevier B.V. All rights reserved.
doi:10.1016/j.enggeo.2011.01.008

based materials, due to its important limitations (Diamond, 2000). Research combining the study of backscattered electron images with the data provided by mercury porosimetry has improved the information about the pore system and the fluid transport phenomena that occur inside the stones (Benavente et al., 2002).

Using the digital image analysis technique on optical or backscattered electron images with different magnification, it is possible to determine the porosity, pore ranges and pore morphologies of the stones (Rogen et al., 2001). However this technique has certain limitations when distinguishing between solid parts (i.e., mineral grains) and empty spaces, and when choosing the most suitable image magnification, as certain magnifications only reveal certain pore sizes (Andriani and Walsh, 2002).

Hydric tests are also important in the characterization of the porosity of stones especially in terms of the movement of water through the "labyrinthine" pore system. They are useful for predicting stone behaviour, as open porosity and the pore system are the main factors controlling water uptake and its transport inside the stone (Vos, 1976; Scherer, 1990; McGreevy, 1996). However, the use of other liquids (i.e., mercury) and gases (i.e., nitrogen) may give us a more complete vision of the pore system.

The instrumental limitations of these techniques when used in isolation lead to incomplete, sometimes ambiguous results. Conversely, the combined use of complementary analytical techniques based both on the direct observation of the pore system (by means of optical and electron microscopy coupled with digital image analysis) and the indirect measurement of the pore system (using hydric tests, mercury intrusion porosimetry and nitrogen absorption) can improve the knowledge in this research field.

Another factor to be taken into account in the study of the pore system is stone durability. In fact, a very common cause of stone deterioration is the formation of ice inside the pore system during freezing. This phenomenon is of great importance in countries where close-to-zero temperature conditions are frequent (Laycock, 2002) and visible frost damage effects have been observed on materials with a porosity of just 5% when saturated in water (Grossi et al, 2007). Soluble salts of various different origins also cause significant decay. Saline solutions can crystallize inside the pores and fissures of a material as subflorescence. This results in the increase of crystallization pressure, causing crack formation and granular disintegration (Steiger, 2005; Espinosa et al., 2008). The use of accelerated decay tests such as the freeze–thaw and salt crystallization tests can therefore provide very useful information about the durability of materials.

To our knowledge there is no study of the pore system of stones that combines the use of all the aforementioned techniques.

This paper has two main objectives. Firstly, to characterize exhaustively the pore system of a set of porous stones in order to predict their physical performance and durability, and secondly to perform accelerated decay tests to assess the effectiveness of petrophysical characterization as a means of predicting the durability of these stones.

The most common kinds of porous rocks are those of a sedimentary nature, many of which have been used since ancient times for construction and ornamental purposes. Sandstone, limestone, dolostone and travertine can be considered as models for other rocks with similar characteristics because of their wide range of porosities, pore types and textures.

2. Materials used

We selected six types of porous sedimentary stones currently quarried in Spain and sold as construction and decorative materials (Table 1).

Santa Pudia limestone (SP, Figure 1a). This is a Tortonian bioclastic calcarenite characterized by an abundance of fragments of bryozoa, red algae, foraminifers, echinoderms and mollusc shells of up to 5 mm in size with a very small amount of siliceous fragments. The matrix of this stone is microsparitic and contains sporadic secondary calcite crystals (Luque et al., 2008). Santa Pudia limestone is the most widely used building material in the historic monuments of Granada.

Fraga limestone (CF, Figure 1b). This is a grey-yellowish micrite-to-biomicrite from the Miocenic Age commonly used in buildings in Aragon and sold under the brand name of "Campanil". It is mainly composed of microcrystalline calcite and very small amounts of quartz, clay minerals and organic matter. Bioclasts are made up of bivalves, charophytes and ostracods (Buj Fandos, 2008).

Boñar dolostone (DB, Figure 1c). This stone comes from the area around the Spanish town of the same name and has been used to build numerous monuments in the north of the Iberian peninsula. It is an Upper Cretaceous grey dolostone with a crystalline texture. Its previous limestone texture underwent a process of dolomitization and was replaced by 30 μm dolomite crystals with a very small amount of quartz grains (Gómez Fernández et al., 2003).

Travertine from Albox (TA, Figure 1d). This is a Pleistocenic, heterogranular, yellow-coloured limestone composed of micritic, sparitic and, above all, fibrous calcite crystals formed from geothermal springs and characterized by large pores. In addition to calcite, sporadic Fe and Mn oxides/hydroxides confer a brownish colour to some of the beds. It is used as an ornamental stone in modern architecture and in restoration work and it is also known by its trade name of "Amarillo Oro" (García Del Cura et al., 2007).

Uncastillo sandstone (AU, Figure 1e). This rock can be classified as a litharenite rich in carbonatic fragments (calcareous sandstone) from the Lower Miocene Age. It has a grain-supported texture with heterogeneous fragments of calcite, quartz, slates and metamorphic rocks with intergranular and syntaxial calcitic cement. Siliceous and carbonatic fragments appear in very similar quantities. Stone fragments are sub-angular to round in shape and generally range between 0.25 and 0.35 mm in size (Buj and Gisbert, 2007). This stone has been used since Roman times, and 80% of the architectural heritage of the Ebro Valley region (Navarre, Aragon and Catalonia) was built with it.

Villaviciosa sandstone (AV, Figure 1f). This is a sublitharenite to subgraywacke rock from the Upper Jurassic Age quarried and used as construction material in the Asturias region and known by its trade name of "La Marina". It has a grain-supported texture and it is composed of quartz grains, feldspar and fragments of quartz-feldspatic rocks with quartz overgrowth cement. Grain sizes range between 0.25 and 0.4 mm (Suárez del Río et al., 2002).

Table 1
Location and main petrographic features of the Spanish lithotypes analysed in this paper.

Trade name	Geographic location	Age	Petrographic type
Santa Pudia (SP)	Escúzar (Granada)	Upper Miocene	Limestone: Biosparite (coarse grain)
Campanil (CF)	Fraga (Huesca)	Lower Miocene	Limestone: Micrite-biomicrite
Boñar (DB)	Boñar (Leon)	Upper Cretaceous	Dolostone: Dolosparite
Amarillo Oro (TA)	Albox (Almeria)	Pleistocene	Travertine: Micrite-sparite
Uncastillo (AU)	Uncastillo (Saragossa)	Lower Miocene	Sandstone: Lithoarenite (calcitic fragments)
La Marina (AV)	Villaviciosa (Asturias)	Upper Jurassic	Sandstone: Subarkose-sublithoarenite

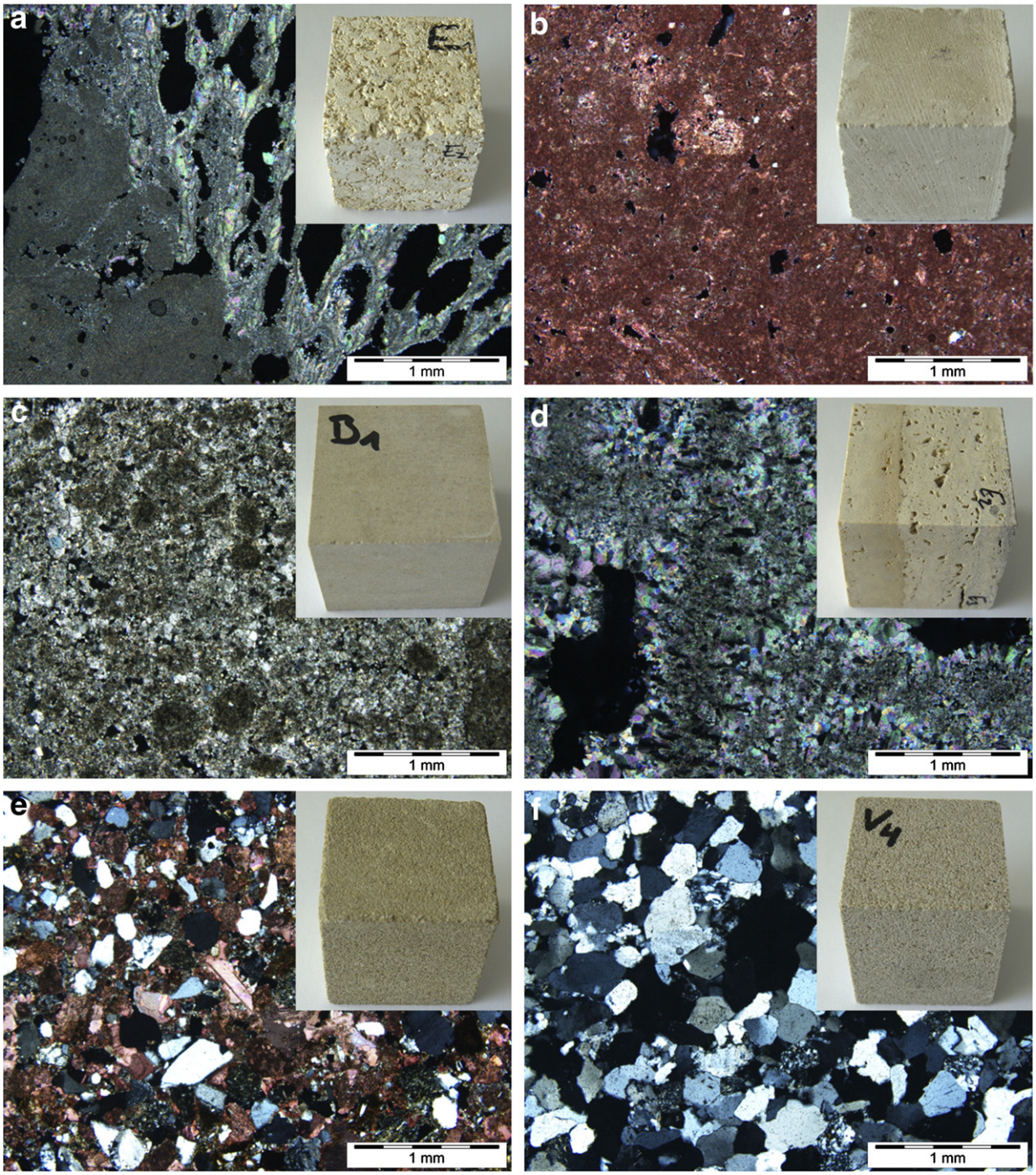

Fig. 1. POM microphotographs showing the mineralogy and pore morphologies of Santa Pudia limestone (a), Fraga limestone (b), Boñar dolostone (c), travertine from Albox (d), Uncastillo sandstone (e) and Villaviciosa sandstone (f). Representative photo of hand specimens are shown as inset in each POM image (each cube is 5 cm-edge).

3. Analytical techniques

3.1. Techniques based on direct observation of pore systems

The texture and microtexture of stones, the morphology and size of the pores, and the existence and distribution of fissures in the stone were analyzed by means of optical microscopy and electron microscopy. Although optical microscopy is the only technique (excluding visual observation) we can use to study the biggest pores (i.e., those of about 1 mm), its low resolution capacity for pores of less than 1 μm is definitely a limitation. This limit can be shifted down to 0.1 μm, approximately, if we examine the samples with a scanning electron microscope (Piekarczyk and Pampuch, 1976). In the case of optical microscopy, we used an Olympus BX60 polarized optical microscope (POM) equipped with a digital microphotography unit (Olympus DP10); the electron microscope we used was a Leo Gemini 1530 field emission scanning electron microscope (FESEM). Two polished thin sections per lithotype were used to show the texture either on two different planes that were, parallel and perpendicular to the bedding plane (when the bedding plane was identifiable) or, more frequently, on two planes perpendicular to each other. Digital image analysis (DIA) was carried out at a magnification of 4× and 20× for POM and 300× for FESEM images and 15 images were taken of each section and analyzed. We chose these magnifications because they covered the

widest range of empty spaces by combining the observation of large pores with a low resolution technique (POM) with the observation of smaller pores that are better recognizable using FESEM. These images were converted to binary by a thresholding process using ImageJ software package (2010): solid parts were displayed in white, while pores and fissures were in black. A Gaussian filter was applied which began by performing an erosion operation. This was followed by dilation, which smoothed the objects and removed isolated pixels. The black pixels were counted and a 2D total porosity and pore size distribution were determined. In order to complete the analysis of samples, another two thin sections per lithotype were impregnated under vacuum using a fluorescent Epoxy SP-115 resin coupled with Epodye colorant. This technique allowed us to obtain a better contrast between empty spaces and solid areas (i.e., crystals). Optical images were binarized and analyzed using the same procedure described above.

3.2. Techniques based on indirect measurement of pore systems

The aforementioned pore size distribution and porosity values were measured again, together with density, using mercury intrusion porosimetry (MIP). For this technique we used a Micromeritics Autopore III porosimeter, model 9410, which can generate a pressure of 414 MPa, covering the pore diameter range from approximately 0.003 to 360 μm. Freshly cut sample chips of about 2 cm^3 were oven dried for 24 h at 100 °C and then analysed. Three MIP measurements were made per lithotype.

The nitrogen adsorption technique was used to complete the micro-mesopore analysis by means of a Micromeritics Tristar 3000 apparatus covering the pore range from 0.002 to 0.05 μm, approximately. N_2 isotherms were obtained at 77 K. BET analysis was used to calculate the specific surface area of the samples, while pore size distribution curves were obtained using the BJH method (Gregg and Sing, 1982).

Similarly, density, porosity and other hydric parameters related to pore morphologies were calculated in order to assess the hydric behaviour of the six types of porous stones. The samples used for these analyses were cube-shaped (5 cm-edge). Four samples were analysed per lithotype. The apparent density (ρ_b), skeletal density (ρ_{sk}) and open porosity (p_o), were calculated (RILEM, 1980) as follows:

$$\rho_b = \frac{M_0}{M_S - M_H};$$

$$\rho_{sk} = \frac{M_0}{M_0 - M_H};$$

$$p_o = \frac{M_S - M_0}{M_S - M_H} \times 100,$$

where M_0 is the mass of the dried sample, M_S is the mass of the sample saturated with water under vacuum and M_H is the mass of the sample saturated with water under vacuum and weighted in water.

To determine these hydric parameters, the samples underwent free and forced water absorptions (EN-13755, 2008) and a drying test (NORMAL 29/88, 1988), covering a pore diameter range from 10^{-2} to 10^3 μm and particularly those below 5 μm (RILEM, 1980). Free water absorption (A_b) (absorption of water at atmospheric pressure), forced water absorption (A_f) (under a vacuum), the degree of pore interconnection (A_x) (Cultrone et al., 2003), the saturation coefficient (S) and the drying index (Di) were measured as follows:

$$A_b = \frac{M_L - M_0}{M_0} \times 100;$$

$$A_f = \frac{M_S - M_0}{M_0} \times 100;$$

$$A_x = \frac{A_f - A_b}{A_f} \times 100;$$

$$S = \frac{M_{48h} - M_0}{M_S - M_0} \times 100;$$

$$Di = \frac{\int_{t_0}^{t_f} f(M_t)dt}{M_S \times t_f},$$

where M_L is the mass of the sample saturated with water at atmospheric pressure (until constant mass is reached), M_{48h} is the mass of the sample after 48 h immersion in water at atmospheric pressure, M_t represents a decreasing water weight content as a function of time and t_0 and t_f are respectively the start and end times for the test.

A capillary test (EN-1925, 2000) was used to determine the capillarity coefficient (C_C) and the capillarity height (H_C). The first value was obtained by measuring the slope of the initial straight line of water absorption curves by capillarity, where M_t is the amount of water absorbed at time t and A is the surface of the sample in contact with the water, while the second value considers the height of water rise by capillarity h at time t:

$$C_C = \frac{M_t - M_0}{A\sqrt{t}};$$

$$H_C = \frac{h}{\sqrt{t}}.$$

In view of the fact that in most of the samples the bedding planes were either not identifiable or poorly defined, we decided to perform the hydric tests with randomly oriented samples.

To complete the study of the movement of water inside the pore system (in this last case in vapour state), we measured the vapour permeability coefficient (Kv) according to the NORMAL 21/85 (1985) standard. This coefficient was obtained by the slope of the straight line of water vapour transfer, where ΔM is the amount of water vapour transfer at time t, and A is the surface of prismatic samples 1 cm thick. Temperature was maintained constant during the test:

$$Kv = \frac{\Delta M / A}{t}.$$

3.3. Accelerated decay tests

Finally, in order to evaluate the durability of the stones and verify the performance levels suggested by the direct observations and indirect measurements of the pore system, we decided to carry out salt crystallization and freeze–thaw tests on the six lithotypes. In the first case, 15 salt crystallization cycles of 24 h each were performed according to the EN 12370 standard (2001) using a solution of 14% $NaSO_4 \times 10H_2O$. This salt is considered a very dangerous contributor to stone decay because of its strong crystallization pressure (Cultrone and Sebastián, 2008). Four samples per lithotype were used. In the second case, 25 cycles of 24 h each were carried out according to the EN 12371 standard (2003) to evaluate how the texture and the pore system were affected by water changing from a liquid to a solid state. Three samples were analysed per lithotype. In both tests, the samples used were cube-shaped (5 cm-edge) and the damage was assessed by a visual inspection of material loss and by measuring weight changes.

4. Results and discussion

4.1. Texture analysis coupled with DIA

Figs. 1 and 2 illustrate the pore system (size, shape, etc.) of the six lithotypes observed by POM and FESEM, respectively. SP limestone shows a high porosity with large pores. The largest pores visible with POM range from 500 μm to 1 mm, although pores of 3–4 mm can be distinguished with the naked eye. Porosity is both intragranular and intergranular, due to the presence of calcified skeleton fragments of red algae and bryozoa, which together with molluscs and foraminifer fragments make up the structure of a poorly cemented stone (Figure 1a). In fact, sparitic calcite fills intergranular pores only sporadically (Figure 2a).

CF limestone shows similar porosity to the previous stone even if the pore sizes are slightly lower. Intergranular and intragranular porosities are due to the presence of fragments of bivalves and charophytes among others (Figure 1b). Pores below 100 μm predominate and the largest measure 500 μm, approximately (Figure 2b).

The low porosity of DB dolostone is a consequence of the dolomitization of a primary calcitic texture. Pores are generally small and do not exceed 100 μm in size (Figure 1c). Moreover, the development of secondary calcite crystals fills some of the pores (Figure 2c).

Two main families of pores can be recognized in TA travertine: one is large, clearly visible to the eye, ranging from 5 mm to 1–2 cm and round to elongated in shape. These pores are of primary origin and are different from the other family, of secondary origin, which is the product of decomposition of organic matter (Figure 1d). In some

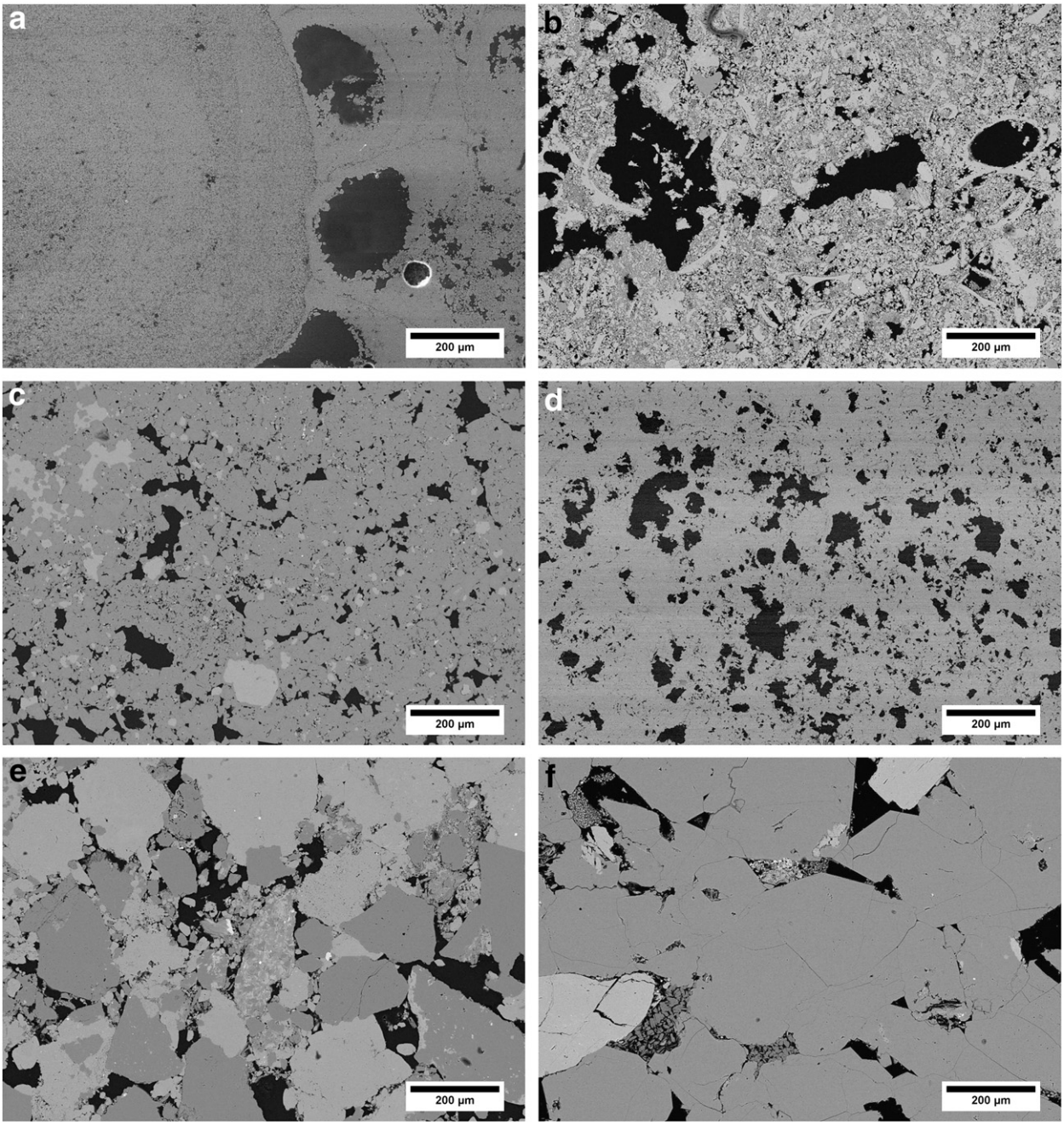

Fig. 2. FESEM images of some microtextures of Santa Pudia limestone (a), Fraga limestone (b), Boñar dolostone (c), travertine from Albox (d), Uncastillo sandstone (e) and Villaviciosa sandstone (f).

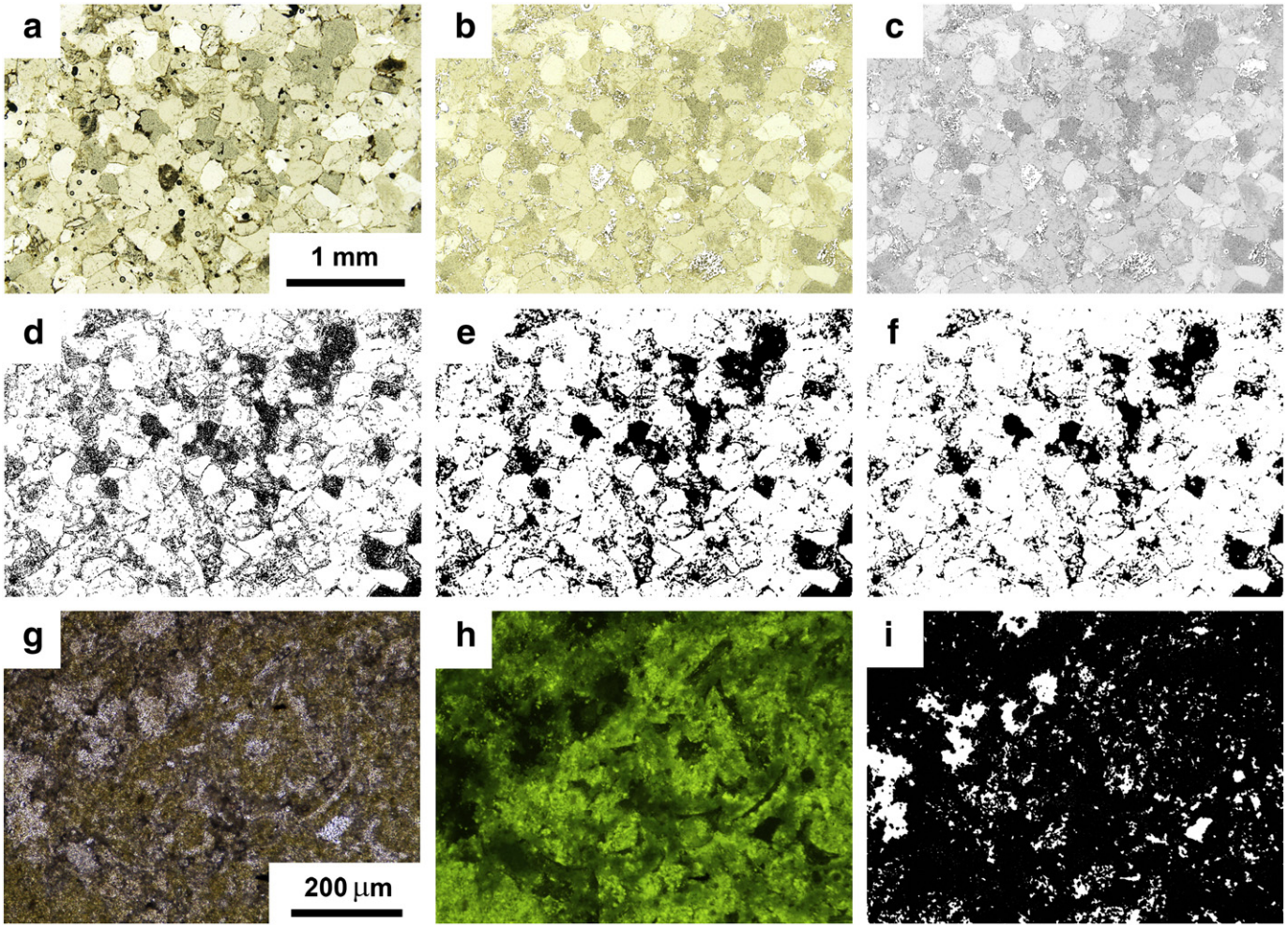

Fig. 3. Examples of DIA process on MOP images. AV sample: (a) original colour image (parallel nicols); (b) colour threshold to erase bubbles and oxide phases; (c) colour change to 8-bit gray scale; (d) binarization; (e) application of smooth and Gaussian blur filter; (f) erosion (pores in black). Micritic CF sample; problems with the use of fluorescent resin: (g) original colour image (parallel nicols); (h) texture of the sample with fluorescence resin; (i) binarization and overestimation of porosity (pores in black).

cases, calcified relicts of original organic textures were detected (Figure 2d).

AU sandstone is characterized by small pores which occupy the spaces between the calcite and quartz grains (intergranular porosity) (Figure 1e). Pore size is below 100 μm and no secondary calcite crystals were detected filling up the pores (Figure 2e).

AV sandstone shows an intergranular porosity (Figure 1f) with pore sizes of approximately 200 μm (Figure 2f), although occasional pores of 700 μm were also detected.

The microphotographs in Fig. 3, the histograms in Fig. 4 and the values in Table 2 show a 2D porosity and pore size distribution recorded on two perpendicular cuts for each lithotype by optical and electron microscopy images after their binarization. The two microscopes identify different pore ranges and porosities in the same stone, especially in the largest and the smallest pore-size regions. Only the combined study of POM and FESEM images can give us a reliable picture of the pore system of the six lithotypes. Of the two procedures (one with fluorescent resin and the other without) used to determine the pore system of POM images, we noted that two lithotypes, DB and CF, provided unsatisfactory results when fluorescent resin was used. This was because of their high content in micrite which did not allow us to distinguish clearly between rock and empty spaces, causing the latter to be overestimated (see Figure 3g–i). The procedure with fluorescent resin was therefore considered an unreliable means of measuring porosity. As a result only un-impregnated samples (without resin) were considered for DIA study. The POM technique was useful for detecting the presence (especially in SP, AU, AV and TA samples) of many pores with a radius of over 100 μm. These pores predominate over the other ranges and strongly affect the porosity value calculated using this method. In the same way, FESEM images improved the identification of pores with radii of less than 50 μm in all the lithotypes (Figure 4). Therefore, in the pore range between 50 and 100 μm, in which the two microscopy observations clearly overlap, we noted a good correspondence in the amount of pores detected by the two microscopes. There was practically no difference between POM and FESEM in the measurement of the pore size distribution of DB and AV stones, and the scattering for the other lithotypes was quite low ranging between 0.3 and 3.6. The exception was SP, which showed more pores in the range of 50–80 μm when using scanning electron microscopy (p was 8.74% with FESEM and 1.21% with POM). The porosity calculated by DIA can be considered as total porosity, because thin sections can show pores that are not in contact with the exterior. The most porous stone is SP (36%, Table 2 and Figure 4), while the least porous is DB (~13%). Fraga limestone (CF) is the rock with the highest number of pores (both open and closed) of less than 10 μm.

4.2. Pore size distribution by MIP and N_2 adsorption

MIP and N_2 adsorption techniques, combined with DIA images provide a more reliable picture of the pore system of the stones. In fact, although the first two techniques analyze 3D porosity and the last only 2D porosity, MIP cannot investigate the shape of pores, because it

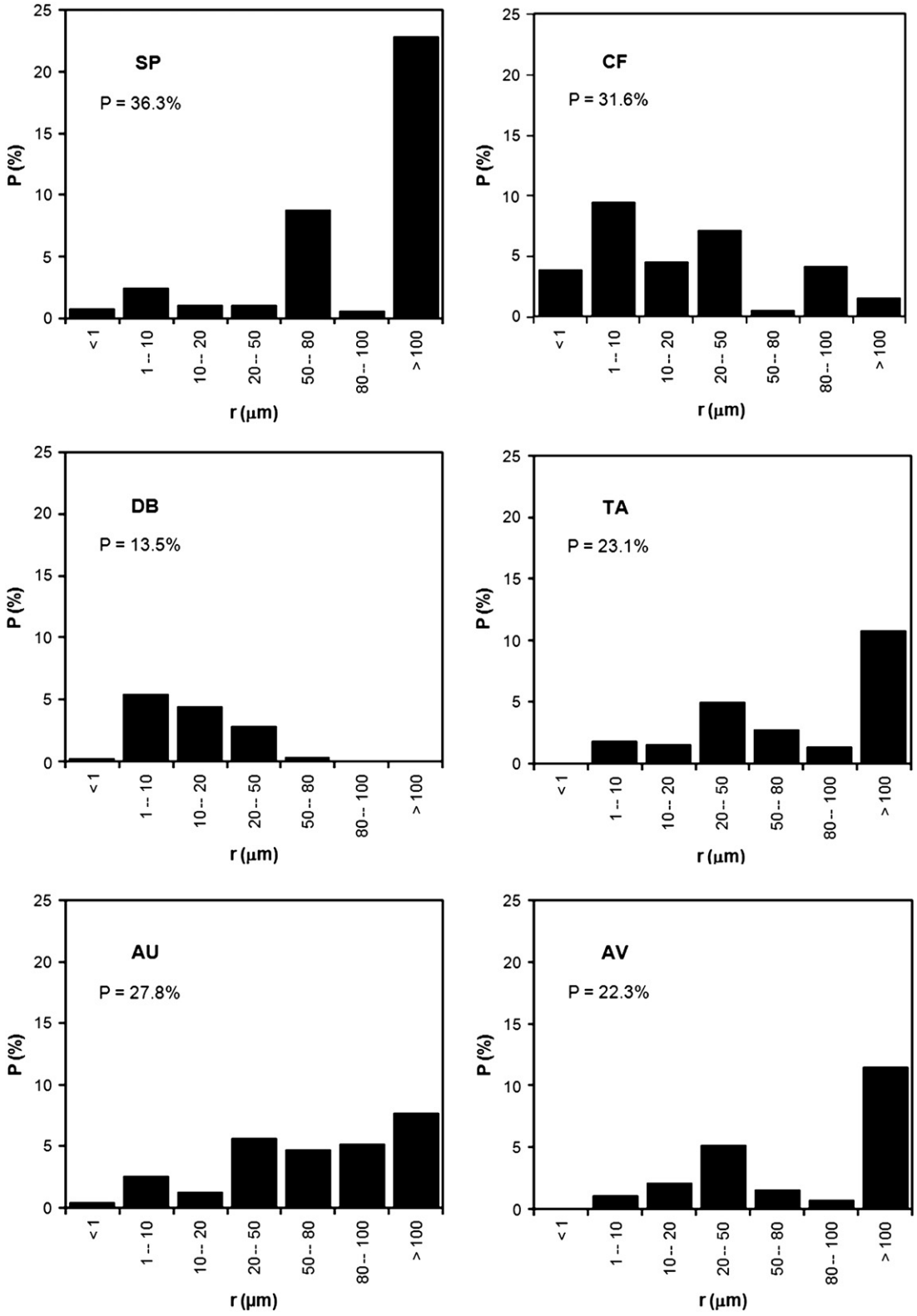

Fig. 4. Pore size distribution histograms and total porosity (P, in %) of Santa Pudia limestone (SP), travertine from Albox (TA), Boñar dolostone (DB), Fraga limestone (CF), Uncastillo sandstone (AU) and Villaviciosa sandstone (AV) after binarization of POM and FESEM images.

views them all as cylinders and does not take into account the fact that some pores are "ink-bottle" shaped. As a result it tends to overestimate the number of small pores. The results provided by these techniques are shown in Fig. 5 and Table 3. Under MIP analysis, SP and TA are the only stones in which the porometric curve shows a bimodal distribution. SP is the most porous stone (33.4%), which confirms DIA measurements. TA, on the contrary, is the least porous stone for the range of pores investigated by MIP, but it is also the one in which the smallest pores predominate (representing more than 20% of its relative porosity). In principle, it would therefore seem very susceptible to decay. In fact, Rodríguez Navarro and Doehne (1999) demonstrated that stones with a high percentage of small pores are

Table 2
Data obtained by direct observation of pore system (POM and FESEM) and image treatment by DIA: p = total porosity (%); distribution of total porosity (%) according to pore sizes ranges (>100, 100–10, 10–1, <1 μm). The value in brackets indicates the amount of relative porosity (%). Stone abbreviations are indicated in Table 1.

Stone	P	>100	100-10	10-1	<1
SP	36.3	21.9 (61)	10.9 (30)	2.5 (7)	1.0 (3)
CF	31.6	1.6 (5)	16.5 (52)	9.5 (30)	4.0 (13)
DB	13.5	0.1 (0.7)	7.6 (56)	5.5 (41)	0.3 (2.3)
TA	23.1	10.8 (47)	10.6 (46)	1.7 (7)	0 (0)
AU	27.9	7.7 (28)	17.0 (61)	2.6 (9)	0.5 (2)
AV	22.4	11.6 (51.8)	9.6 (43)	1.1 (5)	0.1 (0.2)

Table 3
Data obtained by MIP test: ρ_b = apparent density (kg m^{-3}); ρ_{sk} = skeletal density (kg m^{-3}); p_o = open porosity (%); distribution of porosity (%) according to pore sizes ranges (>1, 1–0.1, 0.1–0.01, <0.01 μm). The value in brackets indicates the amount of relative porosity (%). SSA = specific surface area (m^2/g) obtained by N_2 adsorption. Stone abbreviations are indicated in Table 1. Average results for the three samples tested per lithotype.

Stone	ρ_b	ρ_{sk}	p_o	>1	1–0.1	0.1–0.01	<0.01	SSA
SP	1730	2600	33.4	18.5 (55.4)	12.0 (35.9)	1.8 (5.3)	1.1 (3.4)	0.87
CF	1868	2635	29.1	4.3 (14.8)	21.6 (74.4)	3.0 (10.5)	0.1 (0.3)	3.82
DB	2444	2733	9.1	0.6 (6.4)	5.0 (55.5)	3.1 (34.1)	0.4 (4.1)	2.41
TA	2440	2645	7.8	2.1 (25.6)	1.7 (22.4)	2.4 (31.3)	1.6 (20.7)	0.68
AU	2131	2601	18.0	14.0 (77.9)	2.3 (12.6)	1.5 (8.6)	0.2 (0.9)	2.65
AV	2081	2593	19.5	15.6 (81.2)	1.8 (9.3)	0.9 (5.0)	0.9 (4.5)	3.76

more susceptible to salt decay than those with higher amounts of large pores. However, the low open porosity of TA detected by MIP allows only a very small amount of water (and saline solutions) to flow through it compared to the other stones. The same consideration applies to DB in which only 0.6% of its pores measure more than 1 μm, but its open porosity is only 9%.

The other three lithotypes are definitely unimodal, with the main peaks at 0.2 μm in CF (the second most porous rock, almost 30%), at 8 μm in AV and at 11 μm in AU (these two stones have a porosity of around 20%). The pore range values reported in Table 3 show a predominance of large open pore sizes in the calcarenite from Santa Pudia and the two sandstones (Uncastillo and Villaviciosa) compared to the other rocks.

All the porosity values calculated by MIP (p_o) are systematically lower than those determined by DIA (especially in the TA lithotype). This is because DIA can detect very large pores such as those in travertine rocks while MIP cannot detect pores of over 360 μm. This is why there is only a clear correspondence in the porosity values determined by the two techniques in samples with medium levels of porosity (CF and AV).

N_2 adsorption revealed that CF is the stone with the highest amount of the smallest pores (Figure 5). The specific surface area values (SSA, Table 3) are highest in CF and AV. The lowest belong to TA and SP. SSA values do not seem to correlate well with the pore range values listed in Table 3. This is because SSA is mainly influenced by the number of very small pores, which clearly predominate in CF and AV

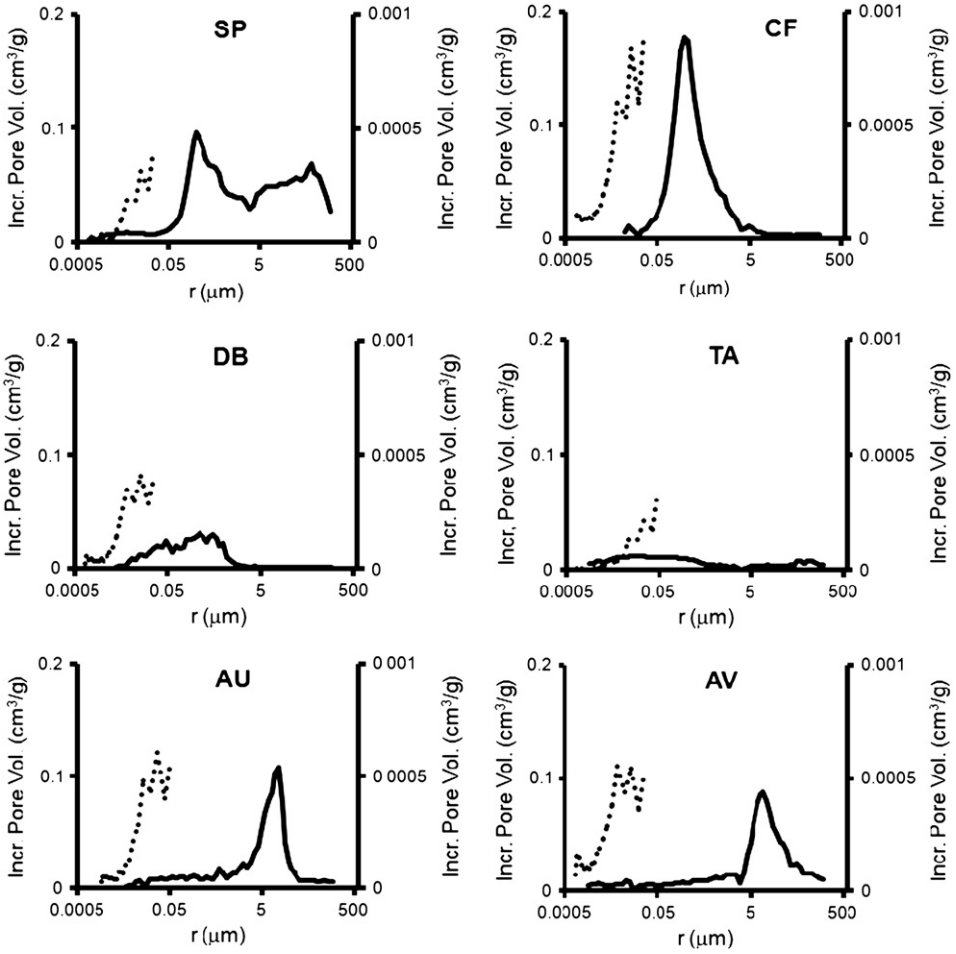

Fig. 5. MIP (continuous line) and BJH (dotted line) pore size distribution curves of Santa Pudia limestone (SP), travertine from Albox (TA), Boñar dolostone (DB), Fraga limestone (CF), Uncastillo sandstone (AU) and Villaviciosa sandstone (AV). Pore radius (in μm) versus Incremental Pore Volume (in cm^3/g) (the left column refers to MIP, while the right to BJH analyses). Each curve shows one of the three measurements made per lithotype.

(see dotted lines in Fig. 5). All of the lithotypes displayed Type II isotherms, which correspond to macroporous materials according to the IUPAC classification (Sing et al., 1985; McNaught and Wilkinson, 1997).

There are some differences between the DIA histograms (Figure 4) and MIP + N_2 adsorption curves (Figure 5), especially in the range of pores with a radius of around 100 μm because it is difficult for the porosimeter to measure pores of this size. In addition it is difficult for DIA to observe pores of around 1 μm. However, over the range 1–100 μm, the profiles drawn by the DIA histograms have the same tendency as the MIP curves, perhaps with the exception of the SP stone.

The skeletal density calculated by MIP (ρ_{sk}, Table 3), is compatible with the mineralogy of the stones. In fact, the highest ρ_{sk} value belongs to DB, which is composed of dolomite, the densest of the minerals that make up these stones (density of dolomite crystal is 2840 kg/m^3). The two limestones (SP and CF) and the travertine (TA) show ρ_{sk} values similar to the density of calcite (2710 kg/m^3). The two sandstones (AU and AV) register the lowest ρ_{sk} value because of the presence of quartz (density of quartz is 2650 kg/m^3), especially in the AV stone.

4.3. Hydric behaviour

Fig. 6 and Table 4 show the hydric behaviour of the six lithotypes. This test shows that the two limestones (SP and CF) absorb much more water (sector 1 in Fig. 6 and A_b value in Table 4) than the other stones, and the travertine (TA) absorbs the least. When the samples were forced to absorb water (sector 2 in Fig. 6 and A_f value in Table 4) we observed how dissimilar the interconnection between the pores in the samples is. TA showed the highest A_x value, as was expected because of its peculiar texture and pore size distribution (Figures 1, 2, 4 and 5), confirming just how difficult it is for water to move through the pore system of a travertine. On the contrary, DB, which is the other least porous stone, has better linked pores (the second best A_x value) which are almost all located in the range 1–0.1 μm (see Figure 5and Table 3). The degree of pore interconnection is an important factor in the ability of stones to dry quickly. If we consider that water plays a part in almost all decay processes (Esbert et al., 1997), the most durable materials will be those that dry out quickly after being wetted. In this case, the worst figures are those measured in the SP and TA samples, even if there are no very marked differences between the six stones (Di).

TA stands out also for its low saturation value (S), i.e. the lowest degree of relative water impregnation, which confirms its low capacity to absorb water. This parameter is clearly linked to pore interconnection (A_x): in fact, the easier the movement of water inside the stones (low A_x values), the higher the S content is. When we compare Ax with MIP pore size distribution curves there is a clear link between the high concentration of pores with a radius of less than 1 μm and the good pore interconnection described by CF and DB samples.

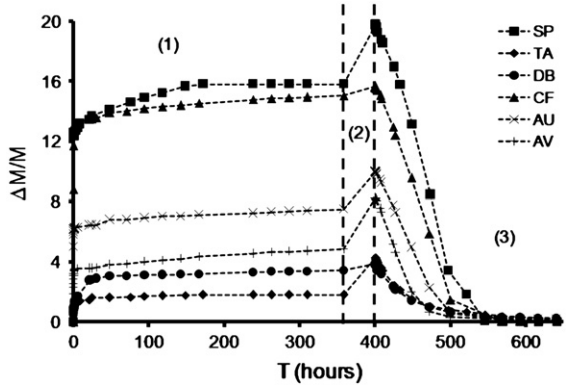

Fig. 6. Free (1) and forced (2) water absorption and desorption (3) curves of Santa Pudia limestone (SP), travertine from Albox (TA), Boñar dolostone (DB), Fraga limestone (CF), Uncastillo sandstone (AU) and Villaviciosa sandstone (AV). Weight variation (ΔM/M) over time (in hours). Four samples were tested for each lithotype. The curves show the average values for the four samples.

Table 4
Data obtained by hydric test: ρ_b = apparent density (kg m^{-3}); ρ_{sk} = skeletal density (kg m^{-3}); p_o = open porosity (%); A_b = free water absorption (%); A_f = forced water absorption (%); A_x = degree of pore interconnection (%); Di = drying index; S = saturation coefficient (%); C_C = capillarity coefficient (g/m^2 s$^{0.5}$); H_C = capillarity height (mm s$^{-0.5}$); Kv = vapour permeability coefficient (g/m^2 × 24 h). Stone abbreviations are indicated in Table 1. Average results for the four samples tested per lithotype.

Stone	ρ_b	ρ_{sk}	p_o	A_b	A_f	A_x	Di	S	C_C	H_C	Kv
SP	1744	2661	34.5	15.8	19.8	20.1	345	71.3	495.6	2.15	273
CF	1870	2640	29.3	15.0	15.7	4.0	314	88.6	171.0	0.76	224
DB	2486	2749	9.5	3.4	3.8	11.1	292	79.2	5.6	0.13	113
TA	2316	2570	9.9	1.8	4.3	58.1	320	37.3	4.7	0.39	47
AU	2116	2683	21.1	7.5	10.0	25.1	306	68.1	201.0	1.43	233
AV	2131	2586	17.6	4.8	8.3	41.5	288	46.1	28.3	0.43	162

Table 5 offers a comparison of the total/open porosity values obtained by DIA, MIP and hydric tests. The open porosity determined by hydric tests is very similar to that determined by MIP and the sample with the highest difference with DIA measurements is again TA, because its pore interconnection is worse than that of the other lithotypes. This may be why TA obtained a lower p_o value with MIP (Andriani and Walsh, 2002). Moreover, even if DIA and hydric analyses manage to investigate pores of 10^3 μm diameter, it is evident that the water in very large pores (i.e. centimetre-sized) will not be retained during absorption and will therefore not be weighed with this test. These pores may however be partially counted by DIA if a part of the pore appears on the edge of the image being studied and is binarized.

The densities calculated with hydric tests (ρ_b and ρ_{sk}) are similar to those calculated by MIP and described in the above section.

The kinetics of capillary imbibition is similar to that of water absorption. Samples absorb water quickly at the beginning of the test. Then, the velocity of capillary rise decreases and stabilizes before reaching an equilibrium value when samples are saturated by water. The pore system of the Santa Pudia limestone (SP) favours rapid water ascent by capillarity (C_C and H_C), because of its large relatively well-connected pores. If we consider the open porosity values determined with MIP and hydric tests, we can see that the highest (SP) and lowest (DB and TA) porous stones are also the lithotypes with the highest and lowest capillary rise. The SP capillarity coefficient is more than twice that of the second highest C_C value (AU stone). We also observed that the two lithotypes with the lowest C_C value (DB and TA) are the only ones in which water rises irregularly and slowly (low H_C values)

Table 5
Comparison of porosity values (in %) for the six lithotypes determined by means of Digital Image Analysis (DIA), Mercury Intrusion Porosimetry (MIP) and hydric tests (HYDRIC). The pore range (in μm) investigated by each method is indicated. Stone abbreviations are indicated in Table 1. The standard deviation of each value is indicated in brackets.

		DIA	MIP	HYDRIC
Stone	Pore range	10^{-1}–10^3	10^{-3}–10^2	10^{-2}–10^3
SP		36.3 (1.1)	33.4 (1.0)	34.5 (0.5)
CF		31.6 (1.4)	29.1 (0.2)	29.3 (0.3)
DB		13.5 (1.1)	9.1 (1.8)	9.5 (0.7)
TA		23.1 (0.2)	7.8 (0.9)	9.9 (0.6)
AU		27.9 (2.0)	18.0 (1.4)	21.1 (0.8)
AV		22.4 (1.2)	19.5 (0.6)	17.6 (0.1)

through the specimens during the capillarity test, because of their low open micro- and mesoporosity and irregular distribution of capillaries.

Finally, as regards water vapour permeability values (Kv), as we might expect, the highest Kv value (270 g/m^2 × 24 h) corresponds to SP, the most porous stone, while the lowest Kv was for TA, one of the two least porous stones and the one with the worst pore interconnection. DB, the other low porous lithotype registered the second lowest Kv value but there was a marked difference between these two values. This is because the pores in the DB stone are much better linked than those in TA (A_x). AV, CF and AU show intermediate values (160 to 230 g/m^2 × 24 h) and in this group there is also a considerable gap between AV and the other two samples due to its very low A_x value.

4.4. Accelerated decay tests

The salt crystallization test (Fig. 7a) had a considerable effect on the Uncastillo sandstone (AU), Santa Pudia limestone (SP) and, above all, Fraga limestone (CF). The weight of these three lithotypes began to increase because of the entry and crystallization of salts in their pore system. The weight increase was higher in the two limestones, which are the two most porous stones. CF was the first stone that started to break, after just 2 test cycles. The loss of weight continued over a number of cycles due to the fact that fragments of an appreciable size broke off. Between the breaks CF stone showed a significant weight increase due to salt crystallization in pores and, probably, in new formed fissures. The other three lithotypes suffered either very little damage (e.g. TA in the 9th cycle) or a progressive but negligible weight increase (DB and AV).

There were some differences in the response of the samples to the freeze–thaw test (Fig. 7b) as compared to the sodium sulphate crystallization test. In general, samples were more resistant to decay and only two lithotypes, SP and CF, clearly broke up (although this only occurred after the 20th test cycle). The rank order of resistance to this decay test was also different, with SP being the least durable stone followed by CF. Therefore, calcarenite was once again the least resistant rock of those studied. The other lithotypes did not show any damage visible to the naked eye after 25 test cycles and experienced only a slight weight increase. The stone whose weight changed the least was the travertine from Albox (TA) followed by DB, AV and AU.

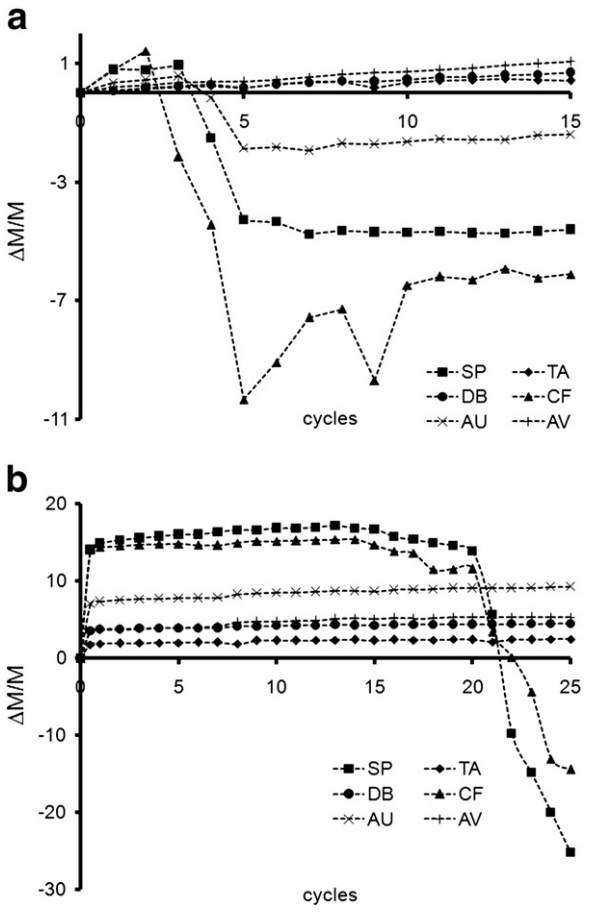

Fig. 7. Weight loss evolution of Santa Pudia limestone (SP), travertine from Albox (TA), Boñar dolostone (DB), Fraga limestone (CF), Uncastillo sandstone (AU) and Villaviciosa sandstone (AV) when submitted to salt crystallization test (a) and freeze–thaw test (b). Each curve shows the average value for the four samples tested per lithotype in the case of Figure "a" and the three samples tested per lithotype in the case of Figure "b".

5. Conclusions

The six lithotypes studied in this work have different textures and, in some cases, different mineralogies. This ensures a wide variability in the porosity (from 10 to 35%, approximately), pore size distributions (unimodal or bimodal curves) and water flow through connected pores and fissures (free water absorption varies from 2 to 16%, approximately). All these parameters were useful to find out more about the pore system of stones and how it can influence their durability.

We observed that the porosity values determined by mercury porosimetry and hydric tests are similar, but lower, than those obtained after binarization of optical and electron microscope images (Table 5) because these techniques focus on different ranges of pores. Moreover, digital image analysis investigates total porosity, while mercury intrusion porosimetry and hydric tests only measure open porosity. The most porous stones are those that absorb most water, even if their ability to absorb water is not always accompanied by a high degree of pore interconnection. Finally, the mineralogical composition influences the density values determined by MIP and hydric tests.

From the data thus obtained and without considering accelerated decay tests, Boñar dolostone (DB) is the rock that almost always achieves the best petrophysical results. This stone shows low porosity, has good pore interconnection, absorbs a low amount of water and dries out fast. Its water ascent by capillarity is also low.

The travertine from Albox (TA) is to some extent similar to the Boñar dolostone because it is the stone that absorbs least water by immersion and by capillarity, and it has low micro- and mesoporosity (even if it has very large pores). However, the stone has a moderate drying speed due to its bad pore interconnection.

The worst parameters were shown by the Santa Pudia limestone (SP) because of its high capacity to absorb water by immersion, and the rapid ascent of water by capillarity. It is the most porous stone and the slowest to dry.

The remaining lithotypes, Fraga limestone (CF), Uncastillo sandstone (AU) and Villaviciosa sandstone (AV), have similar figures as Santa Pudia limestone but better hydric parameters.

Table 6 shows the performance of the six lithotypes on the basis of textural observations coupled with digital image analysis (total porosity), porosimetric and N_2 adsorption analyses (open porosity and specific surface area), and hydric tests (open porosity, degree of pore interconnection, drying index, capillarity coefficient, capillarity height and vapour permeability coefficient). It allocates a score from 1 (highest performance) to 6 (lowest performance) to the six lithotypes and compares the durability assessed according to petrophysical parameters with that measured in accelerated decay tests (salt crystallization and freeze–thaw). The correspondence between the two methods of evaluating durability is evident. The results can be summarized as follows from the most to the least durable stone:

DB—TA—AV—AU—CF—SP.

Table 6
Summary in sketch form of the performance of the six lithotypes predicted by the study of the pore system and the behaviour of these stones after accelerated decay tests. Performance is measured on a scale from 1 to 6 with 1 being the highest and 6 the lowest. Stone abbreviations are indicated in Table 1. The symbols for the DIA, MIP + N_2 and hydric techniques are indicated in Tables 2, 3 and 4 respectively.

	Pore system study											Decay tests		
	DIA	MIP + N_2		Hydric							Mean	Salt	Freeze	Mean
Stone	P	p_o	SSA	A_b	A_x	Di	p_o	Kv	C_C	H_C				
SP	6	6	2	6	3	6	6	6	6	6	5.3	5	6	5.5
CF	5	5	6	5	1	4	5	4	4	4	4.3	6	5	5.5
DB	2	2	3	2	2	2	1	2	2	1	1.9	1	2	1.5
TA	1	1	1	1	6	5	2	1	1	2	2.1	3	1	2
AU	4	3	4	4	4	3	4	5	5	5	4.1	4	4	4
AV	3	4	5	3	5	1	3	3	3	3	3.3	2	3	2.5

The combined use of the aforementioned techniques has allowed a detailed and clear interpretation of the pore systems of the rocks. It corrects misleading interpretations resulting from the limitations of using one single technique and it provides useful information to prevent or to minimize their deterioration. One of the main goals of the improved form of this study is that the durability of the analyzed lithotypes is clearly linked to micro- and mesoporosity, while it is not affected by larger pores (i.e., TA). MIP and hydric tests, although they do not give a complete image of the pore system, are thus more significant with respect to durability of rocks than POM and FESEM. The accurate knowledge of the pore system can allow us to predict the durability (or the quality) of materials subject to the action of decay agents.

Acknowledgements

This study was financially supported by Research Group RNM179 of the Junta de Andalucía and by Research Projects MAT2008-06799-C03 (01, 02 and 03). We are grateful to Nigel Walkington for his assistance in translating the original text. We would also like to thank two anonymous referees for their in-depth reviews.

References

Alonso, F.J., Esbert, R.M., Ordaz, J., 1987a. Caracterización del sistema poroso de calizas y dolomías. Boletín Geologico y Minero 98, 226–237.
Alonso, F.J., Esbert, R.M., Ordaz, J., 1987b. Comportamiento hídrico de calizas y dolomías. Boletín Geologico y Minero 98, 555–576.
Andriani, G.F., Walsh, N., 2002. Physical properties and textural parameters of calcarenitic rocks: qualitative and quantitative evaluations. Engineering Geology 67, 5–15.
Benavente, D., Lock, P., García del Cura, M.A., Ordónez, S., 2002. Predicting the capillary imbibition of porous rocks from microstructure. Transport in Porous Media 49, 59–76.
Benavente, D., García del Cura, M.A., Fort, R., Ordóñez, S., 2004. Durability estimation of porous building stones from pore structure and strength. Engineering Geology 74, 113–127.
Buj Fandos, O., 2008. Caracterización tecnológica de las rocas aragonesas de usos constructivos: propiedades hídricas y durabilidad de las rocas con uso ornamental. PhD Thesis, University of Saragossa.
Buj, O., Gisbert, J., 2007. Petrophysical characterization of three commercial varieties of Miocene sandstones from the Ebro valley. Materiales de Construcción 57, 63–74.
Charola, A.E., 2004. Stone deterioration in historic buildings and monuments. In: Kwiatkowski, D., Löfvendahl, R. (Eds.), Proceedings of the 10th International Congress on Deterioration and Conservation of Stone. ICOMOS Sweden, Stockholm, pp. 3–14.
Cultrone, G., Sebastián, E., 2008. Laboratory simulation showing the influence of salt efflorescence on the weathering of composite building materials. Environmental Geology 56, 729–740.
Cultrone, G., de la Torre, M.J., Sebastián, E., Cazalla, O., 2003. Evaluation of brick durability using destructive and non-destructive methods (DT and NDT). Materiales de Construcción 53, 41–59.
Diamond, S., 2000. Mercury porosimetry. An inappropriate method for the measurement of pore size distributions in cement-based materials. Cement and Concrete Research 30, 1517–1525.
Dunning, J.D., Huf, W.L., 1983. The effects of aqueous chemical environments on crack and hydraulic fracture propagation and morphologies. Journal of Geophysical Research 88, 6491–6499.
EN-12370, 2001. Metodi di prova per pietre naturali. Determinazione della resistenza alla cristallizzazione dei sali. CNRICR, Rome, Italy.
EN-12371, 2003. Metodi di prova per pietre naturali. Determinazione della resistenza al gelo. CNRICR, Rome, Italy.
EN-13755, 2008. Metodi di prova per pietre naturali. Determinazione dell'assorbimento d'acqua a pressione atmosferica. CNR-ICR, Rome, Italy.
EN-1925, 2000. Metodi di prova per pietre naturali. Determinazione del coefficiente di assorbimento d'acqua per capillarità. CNR-ICR, Rome, Italy.
Esbert, R.M., Ordaz, J., Alonso, F.J., Montoto, M., González Limón, T., Álvarez de Buergo Ballester, M., 1997. Manual de diagnosis y mantenimiento de Materiales pétreos y cerámicos. Col-legi d'Apparelladors y Arquitectes Tècnics de Barcelona.
Esbert, R.M., Alonso, F.J., Ordaz, J., 2008. La petrofísica en la interpretación del deterioro y la conservación de la piedra de edificación. Trabajos de Geología 28, 87–95.
Espinosa, R.M., Franke, L., Deckelmann, G., 2008. Model for the mechanical stress due to the salt crystallization in porous materials. Construction and Building Materials 22, 1350–1367.
Franzen, C., 2004. Moisture sorption of natural building stone. In: Kwiatkowski, D., Löfvendahl, R. (Eds.), Proceedings of the 10th International Congress on Deterioration and Conservation of Stone. ICOMOS Sweden, Stockholm, pp. 75–82.
García del Cura, M.A., La Iglesia, A., Benavente, D., Bernabeu, A., González Martín, J.A., 2007. Mineralogía de los travertinos pleistocenos de Albox (Almería), importante recurso de materia prima de rocas ornamentales. Macla 7, 89.
Gómez Fernández, F., Méndez Cecilia, A.J., Bahamonde, J.R., 2003. La Formación Boñar (Cretácico Superior; norte de León): estratigrafía, geoquímica y potencial productor de roca ornamental. Revista de la Sociedad Geológica de España 16, 61–72.
Gregg, S.J., Sing, K.S.W., 1982. Adsorption, surface area and porosity. Academic, London.
Grossi, C.M., Brimblecombe, P., Harris, I., 2007. Predicting long term freeze–thaw risks on Europe built heritage and archaeological sites in a changing climate. The Science of the Total Environment 377, 273–281.
Hall, C., Hoff, W., 2002. Water transport in brick, stone and concrete. Taylor & Francis, Oxon, UK.
ImageJ software package, 2010. Software version 1.43 developed by W. Rasband and freelyavailable from http://rsb.info.nih.gov/ij/index.html, Maryland, USA.
Laycock, E.A., 2002. Ten years of frost testing at Sheffield Hallam University. Construction and Building Materials 16, 195–205.
Lazzarini, L., Laurenzi Tabasso, M., 1986. Il restauro della pietra. CEDAM, Padova.
Luque, A., Cultrone, G., Sebastián, E., Cazalla, O., 2008. Effectiveness of stone treatments in enhancing the durability of bioclastic calcarenite (Granada, Spain). Materiales de Construcción 58, 115–128.
McGreevy, J.P., 1996. Pore properties of limestones as controls on salt weathering susceptibility: a case study. In: Smith, B.J., Warke, P.A. (Eds.), Processes of urban stone decay. Wiley, New York, pp. 150–167. Vol. 4.
McNaught, A.D., Wilkinson, A., 1997. Compendium of chemical terminology, IUPAC Gold Book2nd ed. Blackwell Science.
NORMAL 21/85, 1985. Permeabilità al vapor d'acqua. CNR-ICR, Rome, Italy.
NORMAL 29/88, 1988. Misura dell'indice di asciugamento (drying index). CNR-ICR, Rome, Italy.
Ordoñez, S., Fort, R., García del Cura, M.A., 1997. Pore size distribution and the durability of a porous limestone. Quarterly Journal of Engineering Geology 30, 221–230.
Ordóñez, S., García del Cura, M.A., Fort, R., Louis, M., López de Azcona, M.C., Mingarro, F., 1994. Physical properties and petrographic characteristics of some Bateig Stone varieties. 7th International IAEG Congress Lisbon, Balkema, Rotterdam, pp. 3595–3604.
Piekarczyk, J., Pampuch, R., 1976. Microscopic study of pore structure. Ceramurgia International 2, 177–183.
RILEM, 1980. Recommended tests to measure the deterioration of stone and to assess the effectiveness of treatment methods. Commision 25-PEM: Protection et Erosion des Monuments, pp. 175–253.
Robertson, W.D., 1982. Evaluation of the durability of limestone masonry in historic buildings. In: Brommelle, N.S., Thomson, G. (Eds.), Preprints of the Contributions to the Washington Congress "Science and technology in the service of conservation, pp. 51–55.
Rodríguez Navarro, C., 2003. Análisis porosimétrico de rocas ornamentales. In: Villegas Sánchez, R., Sebastián Pardo, E. (Eds.), Cuadernos Técnicos vol. 8. "Metodología de diagnóstico y evaluación de tratamientos para la conservación de los edificios históricos. Junta de Andalucía, Consejería de Cultura, Granada, pp. 134–153.
Rodríguez Navarro, C., Doehne, E., 1999. Salt weathering: influence of evaporation rate, supersaturation and crystallization pattern. Earth Surface Processes and Landforms 24, 191–209.
Rogen, B., Gommesen, L., Fabricius, I.L., 2001. Grain size distributions of chalk from image analysis of electron micrographs. Computers and Geosciences 27, 1071–1080.
Scherer, G.W., 1990. Theory of drying. Journal of the American Ceramic Society 73, 3–14.
Sing, K.S.W., Everett, D.H., Haul, R.A.W., Moscou, L., Pierotti, R.A., Rouquérol, J., Siemieniewska, T., 1985. Reporting physisorption data for gas/solid systems with special reference to the determination of surface area and porosity. IUPAC. Pure and Applied Chemistry 57, 603–619.
Steiger, M., 2005. Crystal growth in porous materials. I: The crystallization pressure of large crystals. Journal of Crystal Growth 282, 455–469.

Suárez del Río, L.M., Calleja, L., Díez Sarriá, I., Ruiz de Argandoña, V.G., Rodríguez Rey, A., Alonso, F.J., 2002. Características tecnológicas de las rocas ornamentales de Asturias. Trabajos de Geología 23, 73–84.

Vos, B.H., 1976. Water absorption and drying of materials. In: Rossi Manaresi, R. (Ed.), Preprints of the contributions to the International Symposium "The Conservation of stone", vol. II, Bologna, Italy, pp. 679–694.

Vos, B.H., 1978. Hygric methods for the determination of the behavior of stones. UNESCO-RILEM International Symposium "Deterioration and Protection of Stone Monuments", Paris, pp. 1–19.

Whiteley, P., Russman, H.D., Bishop, J.D., 1977. Porosity of building materials — a collection of published results. Journal of Oil and Colour Chemists' Association 60, 142–150.